Influences of recurrence times and fault zone temperatures on the age-rate dependence of subduction zone seismicity

Robert McCaffrey

Department of Earth and Environmental Sciences, Rensselaer Polytechnic Institute, Troy, New York

Abstract. Correlations among subduction zone seismicity, convergence rate and subducting plate age are reassessed considering the possible roles of both recurrence times and fault zone temperatures. Distributions of earthquakes with respect to subducting lithosphere age and convergence rate are grossly explained by a recurrence relation when ages and rates at the world's trenches are taken into account. Correlations between maximum earthquake size M_w^{max} and convergence rate occur because faster subduction lowers the average recurrence time, so that at random within a limited sampling time, faster subduction zones have larger earthquakes. Published empirical slopes of an assumed linear relationship between M_w^{max} and convergence rate are predicted to within 1 standard deviation by such a recurrence model. Recurrence predicts that M_w^{max} should be related to the logarithm of convergence rate and revised age-rate-M_w^{max} data agree with such a relationship. No resolvable global correlation between age and M_w^{max} is found. Hence mechanical explanations of subduction zone seismicity based on such correlations are not required. Predicted average steady state temperatures, based on age and dip of the subducting lithosphere and convergence rate, at most subduction zone thrust faults are within a small range of values ($\pm 50°C$). The few warm outliers, that is, Cascadia, Mexico, and southernmost Chile (south of Chile Rise) that subduct very young lithosphere, also have low seismic coupling coefficients suggesting that high temperature may inhibit seismicity. Fault zone temperatures can explain global variations in seismic coupling coefficients as well as the slab anchor model of *Scholz and Campos* [1995]. Applying this to the Cascadia subduction zone, in contrast to conclusions drawn from mechanical models of subduction and consistent with many other observations, due to its extremely high temperature, Cascadia may be a region where aseismic subduction predominates.

Introduction

Subduction zones are clearly among the Earth's great natural hazards owing to the size of the earthquakes they produce. Quantifying this hazard, however, is elusive because our observations of seismicity are often limited to fractions of the earthquake cycle. Hence we still wonder whether variations in seismic behavior among subduction zones over the past century are characteristic of long-term steady state behavior arising from some physical property of subduction or are simply the present stage of a poorly understood and under sampled cycle of strain accumulation and release. This distinction has practical importance in understanding the earthquake potential of enigmatic subduction zones, Cascadia in particular, where past seismicity gives few clues to its future behavior.

In an attempt to find common characteristics of subduction zone seismicity, *Ruff and Kanamori* [1980] note a linear correlation between the convergence rate at a trench, the age of the lithosphere subducting, and the size of the largest earthquake known to occur near the trench. They conclude that because large and great subduction zone earthquakes during this century occur predominantly where convergence rates are high and the subducting lithosphere is young, fast subduction of

young, buoyant lithosphere creates a shallow trajectory of the subducting plate that enhances stress across the plate boundary [*Uyeda and Kanamori*, 1979]. *Jarrard* [1986] confirmed the age-rate-M_w^{max} relationship but did not find the expected variation in dip angles and questioned the physical model. Nevertheless, the Ruff and Kanamori correlation is used to infer possible maximum size of earthquakes at poorly understood subduction zones, notably Cascadia [*Heaton and Kanamori*, 1984; *Heaton and Hartzell*, 1987], and has since entered textbooks as a fundamental relationship in seismology [e.g., *Lay and Wallace*, 1995]. *Scholz and Campos* [1995] propose a similar mechanical model in which the resistance of the subducting slab to lateral motion through the mantle decreases the normal stress at the plate boundary. They claim that this model, which also predicts a high rate of seismic moment release for Cascadia, is in part validated by and explains global variations with the seismic coupling coefficient.

The purpose of this paper is first to reexamine age-rate-seismicity correlations while taking into account both the nonuniform distributions of ages and rates at the world's trenches and the influence that rate has on recurrence times. It is shown that observed earthquake distributions are strongly influenced by both of these factors, suggesting that faster rate merely reduces recurrence intervals and does not have to involve rate-related physical mechanisms. Then, noting the influence of subducting plate age and convergence rate on temperature of subduction thrust faults, I examine the correlations

of earthquake size and the seismic coupling coefficient with temperature. This work is motivated by the fact that none of the subduction zones included by *Ruff and Kanamori* [1980] and *Scholz and Campos* [1995] to develop their models subduct oceanic lithosphere younger than 20 Ma, while at Cascadia the subducting lithosphere is less than 10 Ma. Because most physical properties of oceanic lithosphere, such as density, temperature, and heat flow, vary with the square root of age, it may not be expected that earthquake size will vary directly with subducting plate age, especially at young ages. Earthquake depths [*Tichelaar and Ruff*, 1993] and agreement between geodetic and thermal models of the locked zone, both at Cascadia and the Nankai trough [*Hyndman et al.*, 1995], suggest that temperature is a useful predictor of the downdip extent of the seismogenic portion of the plate interface and hence may be diagnostic of the potential for a great earthquake. To gain insight into if and how temperature influences seismicity, I estimate fault temperatures at the world's subduction zones based on their convergence rates, dip angles, and subducting lithosphere ages and compare them to earthquake sizes and seismic coupling coefficients. While the correlations by themselves are not compelling, they are no worse than those of the mechanical models, that is, the proposition that high temperature on the thrust fault decreases seismicity is consistent with global subduction zone seismicity variations and with the present quiescence of Cascadia. Hence a thermal explanation of global seismicity variations has very different implications for seismic hazard at warm subduction zones such as Cascadia than do mechanical models.

Data

Several modifications are made to previous compilations [*Ruff and Kanamori*, 1980; *Kanamori*, 1983; *Jarrard*, 1986] of earthquake sizes, subducting plate ages, and convergence rates at subduction zones to account for errors, more recent earthquakes, revised plate motions, and improved age estimates for the subducting lithosphere. I also estimate and use formal uncertainties in the subduction parameters (Table 1). Revisions to the maximum magnitudes of thrust earthquakes were made for the Caribbean, Izu, Ryukyu, and Sumatra because earthquakes other than thrust events were used in the original lists and the Marianas and Java trenches had recent large earthquakes. Dip angles are estimated from mechanisms of thrust earthquakes in the Harvard centroid-moment tensor catalog (HCMT [*Dziewonski et al.*, 1981]) and therefore likely represent the dip angles along the seismogenic plate interface. Estimates of the downdip lengths (*W*) of the active plate interface based on centroid depths of moderate-sized earthquakes are taken from *Pacheco et al.* [1993] and *Tichelaar and Ruff* [1993]. *Hyndman and Wang* [1993] and *Hyndman et al.* [1995] estimate *W* from geodetic data for Cascadia and SW Japan. Two data sets are used to estimate numbers of earthquakes: (1) thrust earthquakes of $M_w \geq 7$ from both *Pacheco and Sykes* [1992] for 1900-1976 and from HCMT for 1977 through April 1996, referred to as the PS7 data set, and (2) thrust earthquakes of $M_w \geq 6$ from HCMT for 1977 through April 1996, called the CMT6 data set. Uncertainties in earthquake magnitudes are assigned based on the year of the event's occurrence (i.e., 1.0 for quakes prior to 1920, 0.5 for those between 1920 and 1960, and 0.2 for those during or after 1960; Table 1).

Convergence rates and subducting lithosphere ages are estimated point-wise along the trenches (Figure 1) (see Appendix for sources of ages and convergence rates) from which averages and standard deviations for each trench are determined (Table 1). Trench lengths are also binned according to age and rate (in 5 Ma and 5 mm/yr bin increments; see Appendix for details). Table 2 shows the discretized distribution of trench length as a function of rate and age that will be used to estimate seismicity as a function of age and rate. Note that the bins are not for contiguous lengths of trench; for example, any particular bin can contain contributions from more than one trench and any trench contributes to a range of bins.

One of the implied assumptions made in earlier analyses is that convergence rates and plate ages are evenly distributed at the world's trenches. However, the binned trench lengths show very peaked distributions (Figures 2a and 2b are histograms of the marginal distributions from Table 2), dominated by convergence rates of 50 to 80 mm/yr and lithosphere of age 10 to 60 Ma (Figures 2a and 2b and Table 2). The peak in age at 100 Ma results from assigning an age of 100±20 Ma to all Cretaceous age seafloor (Appendix).

The numbers of earthquakes in both the PS7 and CMT6 data sets are shown as functions of convergence rate and subducting plate age in Figures 2c through 2f. The PS7 and CMT6 earthquakes are distributed similarly with convergence rate. The distributions with age are also similar except for a large peak in the PS7 quakes at 10 to 15 Ma (all of which are from Mexico and the Central America trenches that have had 33 earthquakes of $7.0 \leq M_w \leq 8.0$ in this century) that does not appear in the CMT6 data. A peak at 100 Ma is relatively higher in the CMT6 data. Figure 3 shows that most earthquakes of $M_w \geq 7$ have occurred where rate is between 50 and 80 mm/yr, mimicking the trench length distribution (Figure 2a). There appear to be more and larger earthquakes at younger ages of lithosphere (<75 Ma, Figure 3b) but again young lithosphere is subducting at most trenches (Figure 2b). As noted also by *Jarrard* [1986], there does not appear to be any direct correlation between earthquake size and dip angle (Figure 3c) as is required in the mechanical models to enhance coupling.

Dependence of Numbers of Earthquakes on Plate Age and Convergence Rate

The world's trenches most commonly have convergence rates of 50 to 80 mm/yr and subducting lithosphere ages of 10 to 60 Ma (Figures 2a and 2b). Hence, if earthquakes are randomly distributed with age and rate, then we expect to find most of them at young ages and high convergence rates, as is seen (Figures 2 and 3). Here I test this supposition but take into account also that faster subduction should result in more and larger earthquakes because it influences recurrence times. To examine the influence of the nonuniform distribution of rates and ages at trenches on the quake distributions, I derive an expression for how the expected number of earthquakes varies with convergence rate and trench length. This procedure also tests whether or not the observed earthquake distribution with age occurs simply because age is also unevenly distributed at the world's trenches.

The number of quakes of seismic moment greater than or equal to M_o is distributed as
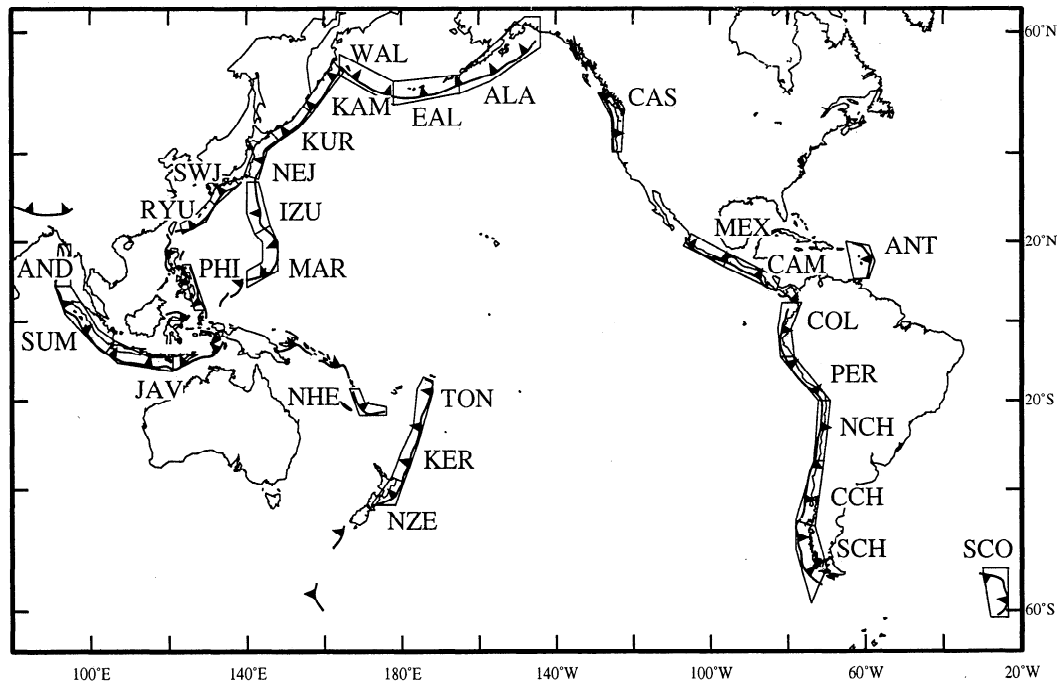
$$N(M_o) = \alpha M_o^{-\beta}$$

Figure 1. Map of world's trenches analyzed in this paper. Each section is labeled with a three-letter code. Geographic limits of trenches and abbreviations are given in Table 1.

for values of M_o less than or equal to some maximum moment M_o^{max} where α and β are constants that depend on frequency-magnitude and moment-magnitude relationships [*Wyss*, 1973; *Richter*, 1958]. *Kagan* [1997] suggests that there is no resolvable variation in β or M_o^{max} among subduction zones, which if true allows the number of quakes above a particular magnitude to be a proxy for moment release. Noting that the seismic moment rate on a fault of length L, downdip width W, rigidity μ and slip rate v is $\mu\, L\, W\, v$, the recurrence interval T for earthquakes of seismic moment M_o or greater is expressed as [*Molnar*, 1979]

$$T(M_o) = \frac{(M_o^{max})^{1-\beta} M_o^{\beta}}{(1-\beta)\ \mu\ W\, v\, L} . \tag{1}$$

Hence the recurrence time for an earthquake of a given seismic moment varies as the inverse of the product of convergence rate and trench length. If the earthquakes are independent in time, the number of expected events of moment equal to or greater than M_o in a given time period τ is τ / T or

$$N(M_o) = \frac{\mu\,\tau(1-\beta)\,W\,v\,L}{(M_o^{max})^{1-\beta}\,M_o^{\beta}} . \tag{2}$$

The conversion from moment to magnitude is

$$M_w = 2/3 \log M_o - 6.0$$

(M_o in Newton-meters [*Hanks and Kanamori*, 1979]). By selecting a value for M_o, (2) becomes $N(v, A)$ because N is a function of v and L, and L is a function of v and A. Using $L = L(v, A)$ from Table 2, (2) predicts the marginal distributions of earthquakes in the PS7 set of $M_w \geq 7$ earthquakes ($M_o=3.5$ x

10^{19} N m; $\tau = 96.6$ years; $W=75$ km; $M_o^{max} =10^{25}$ N m) and in the CMT6 set of $M_w \geq 6$ quakes ($M_o=1.1\times10^{18}$ N m; $\tau = 19.6$ years; $W=75$ km; $M_o^{max} =2.0\times10^{24}$ N m). The values for M_o^{max} were chosen to result in the correct total numbers of events for each group; hence I am testing the distribution of the events with age and rate and not the total number of events. The predicted distributions of earthquakes are shown with solid lines in Figures 2c through 2f.

The distributions of $M_w \geq 6$ and $M_w \geq 7$ events with rate are predicted well using the distribution of convergence rates at trenches (Figures 2c and 2e). Both groups show a small deficit at low convergence rates but the general trends agree well enough that it would be difficult to argue for a rate-dependent difference. Considering that uncertainties in the plate rates are at least a few mm/yr, the excess events in the 80 to 85 mm/yr range satisfy the deficiency in the 70 to 80 mm/yr range. Hence the distribution of the numbers of earthquakes with convergence rate can be explained with a recurrence model and does not require rate-related physical mechanisms [*McCaffrey*, 1994].

The distributions of the numbers of earthquakes with subducting plate age are not as well matched (Figures 2d and 2f). However, considering broad age ranges, the events are distributed correctly between young and old subducting lithosphere. For the $M_w \geq 7$ events, where $A \leq 65$ Ma (57% of trench length), 116 events occurred, while 101 are expected and for $A \geq 100$ Ma (33% of trench length), 57 events occurred, while 60 are predicted. The age range of 10 to 15 Ma has 23 more $M_w \geq 7$ events than expected due to the large number of $M_w <$ 8 earthquakes off Mexico (MEX) and Central America (CAM). Except for MEX and CAM, lithosphere of ages less than 75 Ma shows seismic behavior as expected considering only the distributions of convergence rates and subducting lithosphere ages at the trenches. Hence there is no clear difference in seismicity of old (> 75 Ma) and young (< 75 Ma) subducting lithosphere.

Table 1. Summary of Trench Data

Trench	Code	Minimum to Maximum	RK80 M_w^{max}	K83 M_w'	Age, Ma	Rate, mm/yr	Year	$M_w \pm \sigma_M$ Thrust	M_w All	Length, km	$v \pm \sigma_v$, mm/yr	$v_n \pm \sigma_{vn}$, mm/yr	Age $\pm \sigma_A$, Ma	Dip $\pm \sigma_{dip}$, degrees	No. of dips
Alaska	ALA	195.0°E to 214.8°E	9.2	9.1	40	59	1964	9.2±0.2	9.2	1490	59±6	56±10	49±5	18±7	29
Andaman	AND	9.4°N to 18.8°N			100	20	1978	5.7±0.2	7.7	1089	53±5	12±12	83±4	24±1	2
Antilles	ANT	11.2°N to 19.6°N	7.5	7.5			1982	6.1±0.2	7.2	1227	11±1	9±4	87±6	25±9	17
C. America	CAM	8.3°N to 15.0°N	8.1	8.4	45	80	1950	7.8±0.5	7.8	1506	73±11	72±11	16±1	22±6	54
Cascade	CAS	40.4°N to 49.0°N			20		1992	7.2±0.2	7.6	990	38±5	36±5	5±3	9	1
C. Chile	CCH	-45.4°S to -34.1°S	9.5	9.5	20	111	1960	9.5±0.2	9.5	1306	79±7	71±8	23±9	13±6	3
Colombia	COL	-9.0°S to 2.8°N	8.8	8.8	20	77	1906	8.8±1.0	8.8	1355	69±7	65±8	21±8	22±5	18
E. Aleutian	EAL	178.1°E to 195.0°E	9.1	9.1	60	75	1957	9.1±0.5	9.1	1246	69±6	59±11	56±10	21±6	130
Izu	IZU	23.9°N to 34.2°N	7.2	7.2	150	61	1978	6.6±0.2	7.9	1167	41±6	37±10	145±4	26±6	61
Java	JAV	103.9°E to 130.8°E	7.1	7.1	135	71	1994	7.8±0.2	8.3	3110	75±5	68±8	75±60	20±11	16
Kamchatka	KAM	48.0°N to 54.6°N	9.0	9.0	80	93	1952	9.0±0.5	9.0	900	77±8	74±16	115±35	30±6	97
Kermadec	KER	-38.2°S to -26.0°S	8.1	8.1	120	64	1976	8.0±0.2	8.0	1422	55±8	52±12	100±20	24±7	287
Kuriles	KUR	40.7°N to 48.0°N	8.5	8.8	100	93	1963	8.5±0.2	8.5	1243	81±7	75±14	128±3	26±8	195
Mariana	MAR	11.1°N to 23.0°N	7.2	7.2	150	40	1993	7.8±0.2	7.8	1812	24±7	15±5	134±45	25±8	58
Mexico	MEX	15.0°N to 21.1°N					1985	8.0±0.2	8.0	1383	52±10	49±12	9±3	21±7	18
N. Chile	NCH	-34.1°S to -20.0°S	8.5	8.7	50	110	1922	8.5±0.5	8.5	1579	79±7	74±7	41±4	22±8	78
N.E. Japan	NEJ	35.1°N to 42.8°N	8.2	8.4	130	97	1968	8.2±0.2	8.4	1061	82±8	76±17	132±3	22±7	215
New Hebrides	NHE	-23.2°S to -17.7°S	7.9	7.9	60	27	1980	7.5±0.2	7.9	1189	152±33	111±27	40±8	28±8	96
New Zealand	NZE	-42.8°S to -38.2°S	7.8	7.8	120	55	1931	7.7±0.5	7.7	794	39±5	21±15	100±20	20±10	8
Peru	PER	-20.0°S to -9.0°S	8.2	8.6	45	100	1966	8.1±0.2	8.1	1599	75±7	65±7	37±5	22±8	17
Philippine	PHI	1.1°N to 13.9°N					1972	8.0±0.2	8.2	1509	103±10	72±22	43±27	25±9	149
Ryukyu	RYU	23.0°N to 29.3°N	8.0	8.0	60	56	1986	6.3±0.2	7.6	1153	77±9	68±17	46±13	25±8	31
S. Chile	SCH	-56.2°S to -46.3°S					1983	5.7±0.2	5.7	1218	19±2	16±4	16±6	25	1
Scotia	SCO	-60.7°S to -54.9°S	7.0	7.0	65	20	1987	7.0±0.2	8.0	1005	73±10	44±27	57±29	27±7	86
Sumatra	SUM	-8.0°S to 9.3°N	7.9	7.9	80	66	1984	7.1±0.2	7.8	2462	64±6	50±14	61±10	20±9	98
S.W. Japan	SWJ	29.3°N to 34.0°N		8.6	40	38	1944	8.1±0.5	8.1	824	58±8	53±16	23±1	21±7	10
Tonga	TON	-26.0°S to -14.5°S	8.3	8.3	120	89	1917	8.5±1.0	8.5	1460	184±51	148±64	100±20	24±7	303
W. Aleutian	WAL	164.2°E to 178.1°E					1990	7.1±0.2	7.7	1102	74±6	18±15	72±23	22±8	28

Minimum to Maximum gives the limits of the trench in latitudes if it is a N-S trending trench or in longitudes if it trends more E-W. RK80, *Ruff and Kanamori* [1980] maximum magnitudes; K83, *Kanamori* [1983] adjusted magnitudes; Year is the year of occurrence of the largest thrust event given by M_w thrust; M_w all is the largest event of any type; length is total trench length; v, convergence rate; v_n, trench-normal convergence rate; No. of dips, number of quakes used in the estimate of dip angle.
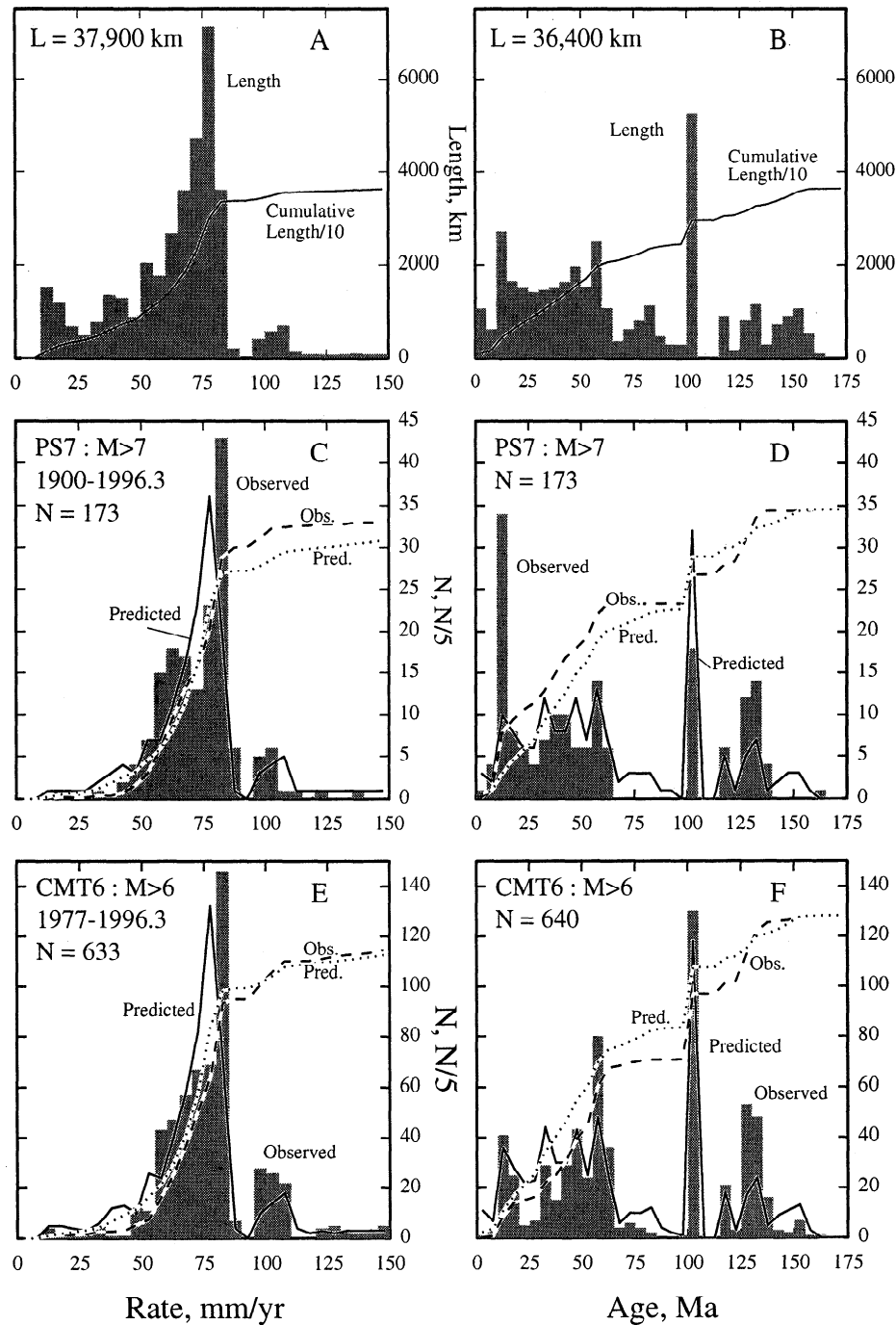
Figure 2. Histograms of the distributions of trench lengths and earthquakes with convergence rates and plate ages. Details of how the histograms are produced are given in the Appendix. The solid lines in Figures 2a and 2b are the accumulated lengths (normalized by 10). L at top is the total length of all trenches in the histogram; these differ between Figures 2a and 2b because some trench sections have unknown ages. Histograms in Figures 2c and 2d show the distributions of 96 years of subduction zone thrust earthquakes of $M_w \geq 7$ (set PS7, see text) and Figures 2e and 2f show 19.6 years of quakes of $M_w \geq 6$ (set CMT6, see text). Solid lines in Figures 2c through 2f are the predicted distributions based on the recurrence model (2). Dashed and dotted lines are the observed and predicted cumulative distributions (normalized by factor of 5), respectively. N within the panel is the total number of quakes in the distribution.

Maximum Earthquake Size and Convergence Rate

It is demonstrated here that the correlation of the size of the largest thrust earthquake M_w^{max} at a subduction zone with convergence rate, found by *Ruff and Kanamori* [1980], *Ka-* *namori* [1983] and *Jarrard* [1986], can be explained by recurrence. They used a relationship of the form

$$M_w^{max} = c_a A + c_v v + c_c$$

where c_a, c_v, and c_c are constants estimated by regression.

Table 2. Trench Lengths Binned by Convergence Rate and Subducting Plate Age

Rate, mm/yr	0	5	10	15	20	25	30	35	40	45	50	55	60	65	70	75	80	85	90	95	100	105	110	115	120	125	130	135	>140	Total
10					77	154	33									220	352	264	209	198										1507
15			402	250	159	48	24													44									242	1169
20	60	44	231																										341	676
25																													473	473
30		105	84																										583	772
35	349	160																			524								319	1352
40	560	66																			307								352	1285
45	11	88	132																		330							99	220	880
50			231	114				36	239							264	605	110	55	44	319							22		2039
55			297	302	114				206		106	95		132	187						330									1769
60			506	262	51					242	870	143		176	110						319									2679
65		22	594	348	311	88	22	66	63	297	200	634	212	55	214	98	168	91	28		99									3610
70				264	84	781	121			79	175	1185	200		102	110					1592								44	4693
75	50	98	121	198	407	253	450	1058	855	447	151	160												901	117				725	5991
80		7	63	318	44	83	187	341	260	131															54	810	1148	167		3613
85	24	18	66	88					10																					206
90																														0
95										44	11	352																		407
100										44		77	407								44									572
105										44			242								44									330
110										55											44									99
115										44											44									88
120										44											44									88
125										44											33									77
>130							623			231											1071									1925
Total	1054	608	2727	1646	1504	1407	1460	1501	1633	1967	1513	2503	1060	363	613	802	1125	465	292	286	5144	0	0	901	171	810	1148	288	3299	36300

Values in table are in kilometers. Numbers on heads for each column or row are the starting value of a bin of width 5; for example 10 means 10 to 15 Ma or 10 to 15 mm/yr. For example, there is 60 km of trench in the world at which the convergence rate is between 20 and 25 mm/yr and the subducting plate age is between 0 and 5 Ma. Each number in bottom row is sum of column above; each number in right column is sum of row to left. These sums comprise most of the histograms in Figures 2a and 2b (sections of trenches where either age and rate are unknown are not included here but are included in Figures 2a and 2b).
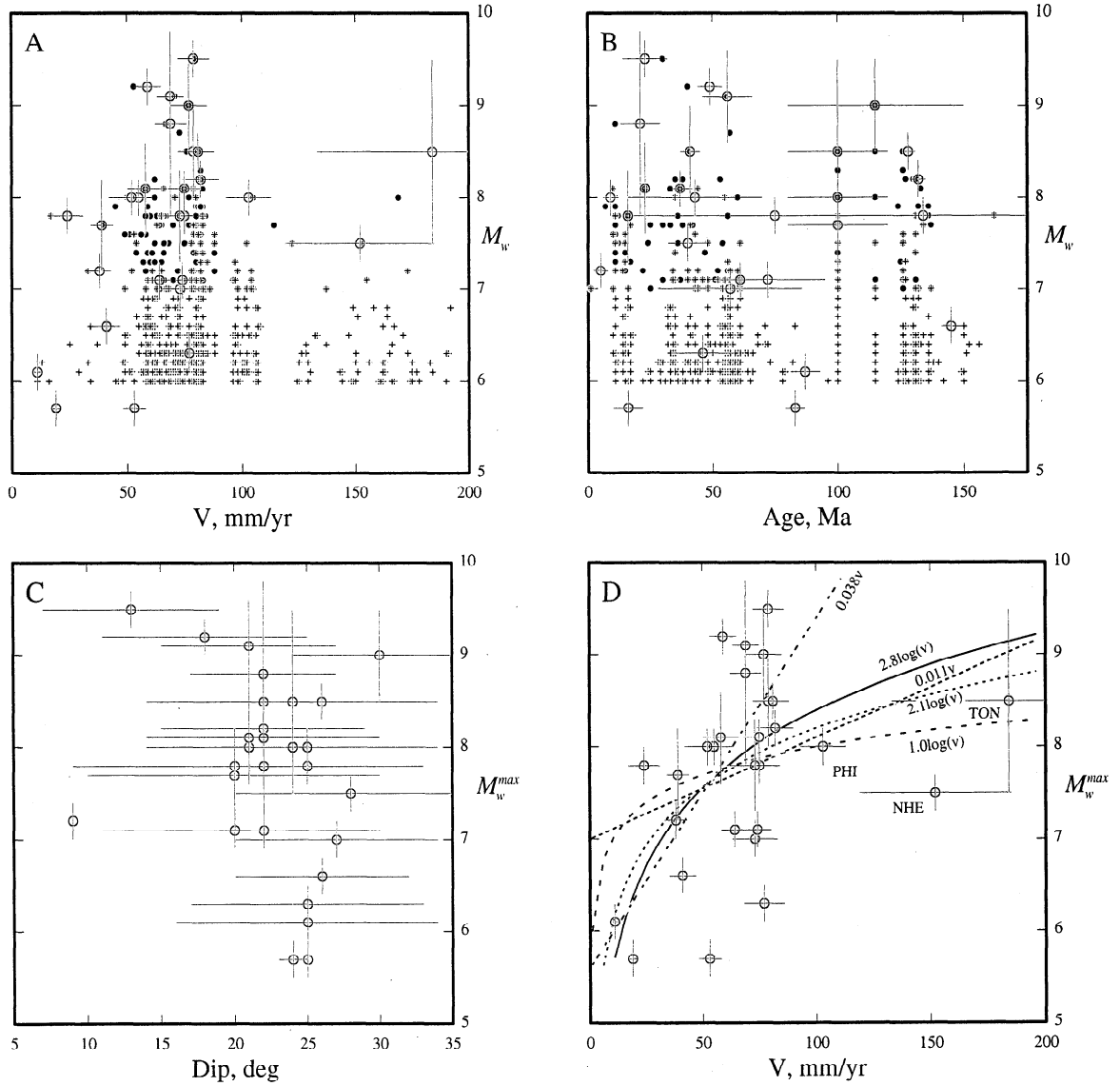
Figure 3. Earthquake magnitudes distributed with (a) convergence rate, (b) subducting plate age, and (c) subducting plate dip angle. (d) Maximum earthquake sizes M_w^{max} at each trench plotted against convergence rate along with linear and log fits as discussed in text. Symbols with error bars are the M_w^{max} at each trench plotted at age and rate averages for the trench (averages and abbreviations from Table 1). Small dots are events from PS7 data and pluses are from CMT6 data, each plotted at their local rate or age. Curves in Figure 3d are labeled according to their convergence rate dependence as described in text and Table 3.

The estimation of statistically significant values for c_a and c_v was used to suggest that the force acting across the plate interface increases with faster convergence and younger plate age [*Ruff and Kanamori* 1980; *Kanamori*, 1983, 1986].

To test the physical interpretation of the rate dependence, the coefficient c_v is estimated from earthquake recurrence. Noting that the larger the earthquake, the less likely it is to occur in some time interval, we can look at "contours" of $T(M_o)$ to see how the seismic moments of earthquakes with equal likelihood (within some time interval) are distributed with convergence rate. Consider earthquakes with a recurrence interval of K, so that $T(M_o) = K$; that is, in the time period K each trench will have the same likelihood of having the earthquake that has a recurrence time of K. According to (1), the moment of this earthquake will be larger for trenches with

faster subduction. Setting $T(M_o) = K$ and solving (1) for M_o gives

$$M_o^\beta = \frac{K(1-\beta)\,\mu\,L\,W\,v}{(M_o^{max})^{1-\beta}}$$

Replacing M_o with M_w as above, taking the logarithm of both sides, and solving for M_w gives

$$M_w = \frac{2\log(C\,v)}{3\beta} - 6.0$$

$$C = \frac{K(1-\beta)\,\mu\,L\,W}{(M_o^{max})^{1-\beta}} \quad . \tag{3}$$

The theoretical value for c_v (the change of M_w with convergence rate) is then

$$c_v = \frac{dM_w}{dv} = \frac{2}{3\beta \ln(10)} \frac{1}{v} = \frac{0.290}{\beta v} \quad (4).$$

The observed largest earthquake M_w^{max} at any trench in any given time period can be represented by $M_w \pm \Delta M_w$; where M_w is derived from (3). If ΔM_w is random then the slope of M_w^{max} (v) will be the same as c_v in (4). The expression for c_v has v-dependence ($1/v$ form) so the straight-line slope derived from such data will depend strongly on the values of v used. Here the theoretical value of c_v is estimated by calculating M_w using (3) for each trench (using L, W, and v from Table 1; $K = 96.3$ years) and finding the slope of M_w with respect to v by regression (c_v and c_a are largely independent shown by a small covariance).

The theoretical slopes estimated in this way compare well to the observed slopes for the *Ruff and Kanamori* [1980], *Kanamori* [1983], and *Jarrard* [1986] regressions (Table 3). In one trial, the *Kanamori* [1983] data are weighted by the inverse of the sum of the squares of the uncertainties in age, rate, and M_w^{max} (estimated for the revised data). Weighting changes the relative importance of the trenches in the regression which in turn affects the slopes slightly, but still the theoretical and calculated slopes agree. The revised data show less agreement between observed and expected values of c_v, probably because the new rates, that include rapid subduction at New Hebrides (NHE) and Tonga (TON) span nearly twice the range of the *Kanamori* [1983] data. When observations are not weighted by uncertainties, the coefficients are strongly influenced by NHE and TON that have large convergence rates (Figure 3d), giving $c_v = 0.011$. When weighted by the uncertainties, NHE and TON, with large uncertainties, have less influence on the solution and a larger c_v is found (0.038). If NHE and TON had lower convergence rates, as in the *Kanamori* [1983] data, M_w^{max} would appear to be much more linear in v.

Equation (3) suggests that M_w^{max} should be proportional to $\log(v)$ rather than to v. Using an equation of the form

$$M_w^{max} = c_a A + c_v \log(v) + c_a$$

fits the data with 12% less misfit variance than the linear relationship for unweighted data (Table 3). For weighted data, the $\log(v)$ equation gives a 6% poorer fit. The data from NHE and TON are visually better explained by the $\log(v)$ relationship (Figure 3d) but the large uncertainties in their ages and rates cause them to have little influence in the weighted solution. Thus whether or not the $\log(v)$ relationship is the better one depends on the faith one puts in data from those two trenches. The expected coefficient c_v for the $\log(v)$ relationship is 1.0 if $\beta = 2/3$ [*Rundle*, 1989] (equation 3). The computed best fit coefficients are between 2.1 ± 0.7 (unweighted) and 2.8 ± 0.5 (weighted), within a few standard deviations of 1.0, which itself gives an acceptable match to the data (Figure 3d). If there is any tendency in the v - M_w^{max} data with respect to the expected $\log(v)$ relationship, it is for the largest quakes to occur at rates between 60 and 80 mm/yr. Within this rate range the observed M_w^{max} vary by about 1.5 magnitude units from their predicted values. In conclusion, the dependence of maximum earthquake sizes on convergence rates at trenches is similar to that expected from consideration of recurrence times only (if $\Delta M_w \approx 1.5$) and additional convergence rate related mechanisms are not required.

The revised data show no direct dependence of M_w^{max} on plate age (Figure 3b); that is, the regression values of c_a are not significantly different from zero for either linear or log relationships (Table 3). Lithospheric buoyancy [*Kanamori*, 1983] and thrust fault temperatures (discussed below) suggest that earthquake size may scale with the inverse of the square root of age. However, using the relationship

$$M_w^{max} = c_a A^{-1/2} + c_v \log(v) + c_c$$

in the regression again results in unresolved non-zero values for c_a (Table 3).

Earthquake Size and Temperature on the Thrust Fault

The foregoing treats lithosphere age and convergence rate as independent in their impacts on seismicity. Moreover, the regressions are dominated by the majority of subduction zones that have moderate convergence rates and ages. One way that age and rate are related is through their influence on the temperature on the thrust fault [*Molnar and England*, 1995]. Temperatures at and near the plate interface may influence earthquake size by controlling the maximum depth of seismic

Table 3. Summary of Fits to Age-Rate- M_w^{max} Data

Data Used	Number of Trenches	c_v Fit, M_w per mm/yr	c_v Theory, M_w per mm/yr	c_a Fit, M_w per Ma	c_c Fit	Misfit Variance
Ruff and Kanamori [1980]	21	0.013±0.004	0.011±0.002	-0.008±0.002	7.9±0.3	0.20
Kanamori [1983] (no uncertainties)	22	0.015±0.003	0.010±0.001	-0.009±0.002	8.0±0.3	0.16
Kanamori [1983]: (with uncertainties)	22	0.011±0.002	0.010±0.001	-0.012±0.002	8.5±0.3	0.14
This paper: linear (no uncertainties)	28	0.011±0.005	0.006±0.001	-0.001±0.004	7.0±0.5	0.97
This paper: linear (with uncertainties)	28	0.038±0.006	0.015±0.001	-0.005±0.003	5.6±0.3	0.80
This paper: log(v), no uncertainties	28	2.1±0.7	1.0	0.000±0.004	6.1±0.6	0.85
This paper: log(v), with uncertainties	28	2.8±0.5	1.0	-0.002±0.003	5.6±0.4	0.85
This paper: log(v), $A^{-1/2}$, no uncertainties	28	2.1±0.7	1.0	0.5±2.1	4.0±1.4	0.85

In the regressions, rates (in mm/yr) and ages (in megaannum) were divided by 10 to make their uncertainties of the same order of magnitude as those of the magnitudes. The coefficients here are corrected to remove the normalizations. Weighting of each observation is by $(\sigma_M^2 + \sigma_v^2 + \sigma_A^2)^{-1}$ (Table 1). Coefficients estimated by *Jarrard* [1986] ($c_v=0.0159$, $c_a=0.0105$, $c_c=8.01$) do not differ significantly from those of *Kanamori* [1983].

slip (i.e., the downdip width W of the seismogenic zone) [*Tichelaar and Ruff*, 1993; *Hyndman and Wang*, 1993]. Higher temperatures may inhibit seismic slip by causing stable sliding in the thrust zone [*Tse and Rice*, 1986; *Scholz*, 1990] and by promoting anelastic strain or intraplate quakes in the upper and lower plates that dissipates strain energy that is otherwise released in subduction thrust earthquakes. Temperature, as a possible control on seismicity, will have particular relevance to the Cascadia subduction zone which is quite hot [*Hyndman and Wang*, 1993]. Here I estimate temperatures of the world's subduction thrust faults based on age, rate, and dip angles and compare these temperatures to observed earthquake behavior.

In the absence of shear heating and crustal heat production, the steady state temperature T_f on a thrust fault subducting oceanic lithosphere of age A at a trench-normal convergence rate v_n is [*Molnar and England*, 1995]

$$T_f = \frac{1}{S}\frac{T_o z_f}{\sqrt{\pi\kappa(A+t_1)}}, \quad S = 1+b\sqrt{\frac{v_n z_f \sin\delta}{\kappa}} \quad (5)$$

where T_o is the initial temperature of the half-space (mantle asthenosphere), z_f is depth on the fault, κ is thermal diffusivity, $t_1 = z_f / (v_n \sin \delta)$ is the time for the lithosphere to subduct to depth z_f ($A+t_1$ is the age at z_f), b is a constant close to unity, and δ is the dip angle. This equation describes the thermal consequences of advection of the oceanic lithosphere beneath the forearc. In this formulation the oceanic lithosphere has a thermal structure governed by its age, 0°C at the top and $T(z) = T_o$ erf [½ z $(\kappa A)^{-\frac{1}{2}}$], where z is depth into the cooling half-space and erf is the error function [*Carslaw and Jaeger*, 1959]. The heat flux through the top of the oceanic lithosphere is $kT_o(\pi\kappa A)^{-\frac{1}{2}}$, where k is the thermal conductivity of the lithosphere. Thus the younger the lithosphere, the higher the heat flux. However, if the subduction rate is fast (S is large) then the fault remains cooler because the temperature at the base of the hanging wall is more influenced by the cold, top surface of the subducting lithosphere than by the warm interior.

Figure 4 shows contours of the average steady state temperature on the thrust fault from 10 to 60 km depth below the seafloor as a function of subduction age and rate, for dip angles of 15° and 25°, derived from (5) (because T_f is nearly linear with z; this is also the approximate temperature at 35 km depth on the fault). The limits of the fault are taken at 10 km depth because the upper 10 km or so of subduction zones are generally aseismic [*Byrne et al.*, 1988], and at 60 km which is the downdip end of seismicity on the thrust interface seen globally [*Pacheco et al.*, 1993]. Frictional heating will produce a convergence rate-related temperature increase of $\Delta T_f = \sigma v_n z_f (Sk)^{-1}$ [*Molnar and England*, 1995], where σ is the shear stress. Heating due to 20 MPa of shear stress on the fault (a best estimate of the global average by *Tichelaar and Ruff* [1993] and *Peacock* [1996]) varies from tens of degrees at low convergence rates to over 100°C at high rates (Table 4). Also, heating due to 20 MPa of shear stress roughly offsets the cooling due to advection and temperatures become independent of convergence rate when young lithosphere is subducting (Figure 4c). Because the magnitude of the shear stress is poorly constrained, it is clear that we cannot in this simple way make accurate estimates of the actual temperature at subduction zones. Nevertheless, the relative temperatures should
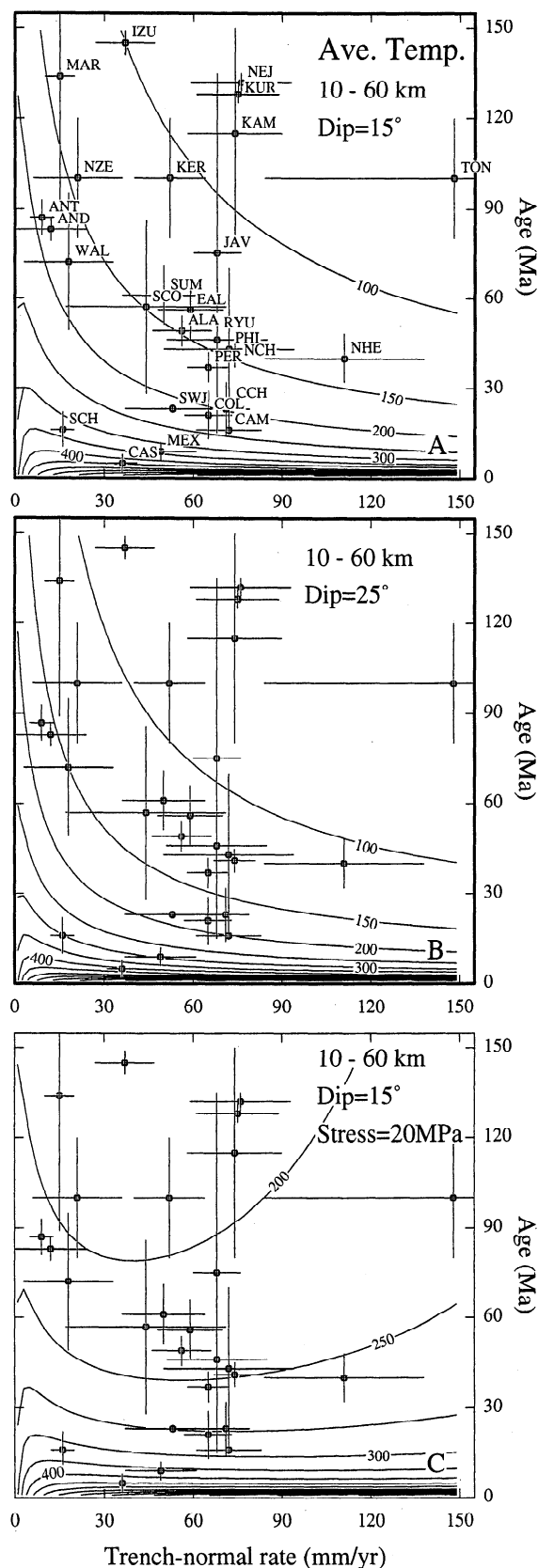

Figure 4. Contours (labeled in °C) of the calculated average temperature on a dipping thrust fault from 10 to 60 km depth as a function of plate age and trench-normal convergence rate (5). Each trench is plotted at its position in age-rate space (Table 1). Figures 4a and 4b are for different dip angles and Figure 4c includes heating from 20 MPa of shear stress. Three-letter codes given in Table 1.

Table 4. Observed and Estimated T and W

Trench	W, km (TR)	W, km (PS)	W, km (HW)	T_1, °C	W_1, km	T_2, °C	W_2, km	χ
ALA	139	113		139	165	230	165	0.77
AND		150		162	125	208	125	0.01
CAM		93		203	136	300	93	0.07
CAS			80	435	65	528	28	0.01
CCH	123	88		129	136	227	136	0.55
EAL	108	94		122	142	210	142	0.84
JAV		130		102	149	199	149	0.01
KAM	129	97		70	102	158	102	0.82
KER		97		91	125	171	125	0.15
KUR	144	82		69	116	162	116	0.38
MAR		74		120	121	168	121	0.01
MEX	58	65		296	103	377	55	0.37
NEJ	196	109		72	136	171	136	0.21
NHE		66		106	109	220	109	0.13
PER	149			141	136	233	136	0.02
SCO		53		123	112	193	112	0.01
SUM		150		126	149	209	149	0.05
SWJ			150	192	142	276	117	1.00
TON		68		63	125	204	125	0.66
WAL		53		158	136	210	136	0.57

W estimates from *Tichelaar and Ruff* [1993] (TR), *Pacheco et al.* [1993] (PS) and [*Hyndman and Wang*, 1993; *Hyndman et al.* 1995] (HW). T_1 and W_1 are calculated average temperature and downdip width of thrust between 10 and 60 km depth without shear heating. T_2 and W_2 are the same but with heating from 20 MPa of shear stress on the fault. χ is the seismic coupling coefficient.

be useful unless the shear stress is high and variable among subduction zones, but there is little evidence to support such a possibility [*Peacock*, 1996]. Radiogenic heating will produce a temperature increase of less than 20°C [*Tichelaar and Ruff*, 1993] and is ignored here.

Figure 4 demonstrates that when the lithosphere is younger than about 30 Ma, subducting plate age has a profound impact on temperatures and that most subduction zones probably have very similar temperatures despite their differences in age and rate. That the range of observed convergence rates at the world's trenches produce relatively small temperature variations is consistent with the point made earlier that seismicity variations due to convergence rate are largely explainable by recurrence times.

Although Cascadia (CAS), Mexico (MEX), and south Chile (SCH), that have not had known subduction earthquakes in excess of magnitude 8, are similar in age and rate to Central Chile (CCH), SW Japan (SWJ), and Colombia (COL), that have had great earthquakes, the differences are at young ages and have significant thermal consequences (Figure 4a). For example, Cascadia is on average more than 200°C warmer than Central Chile (Table 1) largely because its subducting lithosphere is half as old. All of the trenches studied by *Tichelaar and Ruff* [1993], except Mexico, revealed a maximum depth of seismicity of around 50 km. Mexico's maximum depth of 25 km is consistent with inferences from the thermal calculations that it is significantly hotter than the others. The maximum depth of interplate seismicity is unknown at Cascadia and south Chile.

If earthquakes do not occur on the thrust fault where it exceeds some limiting temperature T_c then we can estimate W as a function of plate age and rate by setting $T_f = T_c$ and $z_f = W \sin \delta$ in (5). This limiting temperature is probably between 250°C and 400°C [*Tse and Rice*, 1986; *Tichelaar and Ruff*, 1993]. *Tichelaar* [1991] concludes that coupling depth does not correlate with age and rate, but this is based on a few comparisons at ages greater than 20 Ma (at this age the temperatures are not as dependent on age as they are for younger subducting lithosphere). Using (5) and $T_c = 350$°C, both the average temperature on the thrust and W are calculated for each trench from the estimates of dip angle, plate age, and trench-normal convergence rate (Table 4). In general, some agreement between thermal estimates of W and those from earthquake depths and geodetic data is evident (Figure 5a), suggesting that W may be thermally controlled. In addition to decreasing W, temperature might limit earthquake size also by changing mechanical properties of the fault surface that may decrease the amounts of seismic slip and along strike slip propagation. For example, high temperature promotes ductile shearing at the expense of frictional behavior and lowers the shear stress on the fault [*Stesky et al.* 1974]. However, comparing calculated temperatures (Figure 5b) and W (Figure 5c) to M_w^{max} is less conclusive possibly because most subduction zones are nearly the same temperature and because great earthquakes probably saturate the downdip dimension of the thrust fault [*Scholz*, 1990]. The few thermal (hot) outliers have only earthquakes of $M_w \approx 8$ or smaller, but many cooler subduction zones show this feature as well. Statistically, there is a 30% chance that the maximum earthquake sizes at the three hottest subduction zones represent a random sampling of all subduction zones. In conclusion, temperature appears to be a useful predictor of W but not of M_w^{max}, probably owing to factors other than W that contribute to maximum earthquake size.

Seismic Coupling Coefficients and Temperature

The ratio of the observed to expected seismic moment release on a fault is known as the seismic coupling coefficient (χ) and is often used as a measure of the seismic behavior of a fault. χ has been correlated with other subduction zone parameters to gain insight into the physics of subduction [*Peterson and Seno*, 1984; *Pacheco et al.*, 1993; *Scholz and Campos*, 1995]. The total seismic moment for any given region is typically dominated by the largest event which contributes 20% to 40% of the moment [*Peterson and Seno*, 1984] making χ unstable through time [*McCaffrey*, 1997]. Not surprisingly, χ and M_w^{max} are strongly correlated [*Pacheco et al.*, 1993] but using χ instead of M_w^{max} as the measure of seismic coupling has the possible advantage that it can account for more than one large event.

Scholz and Campos [1995] present a mechanical model for subduction in which the subducted slab dragging through the mantle is pulled downward, lowering the normal stress across the thrust fault at the plate boundary above. The decrease in normal stress should promote stable sliding on the plate boundary and a decrease in χ. *Scholz and Campos* [1995] show that a large inferred decrease in the normal stress across the plate interface corresponds with low χ, while a small decrease in the normal stress produces a low or high χ (i.e., only the combination of high decrease in the normal stress and high χ are excluded; Figure 6a).

Due to the possible thermal effects on slip stability, the seismic coupling coefficient might also be expected to decrease with higher temperature. Comparing the calculated average temperature at subduction zones to χ inferred from earthquakes in this century only (see Appendix) shows similarity to the variation of χ with change in normal stress, in that high temperature and high χ are excluded (Figure 6b). Neither

of the mechanisms provide a statistically robust explanation of the seismic coupling coefficients. In the slab drag mechanism (Figure 6a) there is a 5% chance that the five points with high decrease in normal stress and low χ ($\Delta F_n > 3$, $\chi < 0.2$) comprise a random sample of the total population of χ. Moreover, the five points come from only two contiguous subduction zones (Izu-Mariana and Tonga-Kermadec-New Zealand). If these are used as two subduction zones, then the chance of randomness is 24%. In the thermal model (Figure 6b) there is a 32% chance that the three warm ($T > 250°C$, $\chi < 0.4$) subduction zones are randomly drawn from the global χ population. Hence, to the degree that χ is a useful measure of long-term seismic behavior, the slab anchor and thermal models have similar success in explaining its global distribution. Yet, the two concepts make very different predictions for the seismicity of warm subduction zones such as Cascadia.

Implications for the Cascadia Subduction Zone

Mechanical models for subduction zones are used to predict a high degree of coupling for Cascadia [Heaton and Kanamori, 1984; Scholz and Campos, 1995] yet the seismic quiescence of Cascadia remains inconsistent with such models. The 1992 M_w=7.2 Cape Mendocino quake may [Hagerty and Schwartz, 1996] or may not [Tanioka et al., 1995] have been on the plate boundary but in any case would account for little of the expected seismic moment. Buried coastal marshes and associated sand layers have been interpreted as evidence that Cascadia ruptures in great thrust events every few hundred years [Atwater, 1992; Nelson et al., 1995]. Recent thermal and dislocation models of the Cascadia subduction zone suggest that the downdip extent of the cool and presumably seismogenic portion of the plate interface is small but not insignificant [Hyndman and Wang, 1993, 1995] and a $M \approx 9$ earthquake could occur if the entire 1000 km length of the subduction zone ruptured.

Cascadia has a long stretch of slowly subducting, very young lithosphere (Figure 7) producing to a warm plate interface. Moreover, the newly formed oceanic lithosphere is blanketed with sediments that keeps its surface warm, estimated at about 250°C as it enters the subduction zone [Hyndman and Wang, 1995]. Other trenches that have estimated temperatures relatively close to that of Cascadia are Mexico and South Chile. The South Chile subduction zone is also largely void of seismic moment release. The HCMT catalog contains only
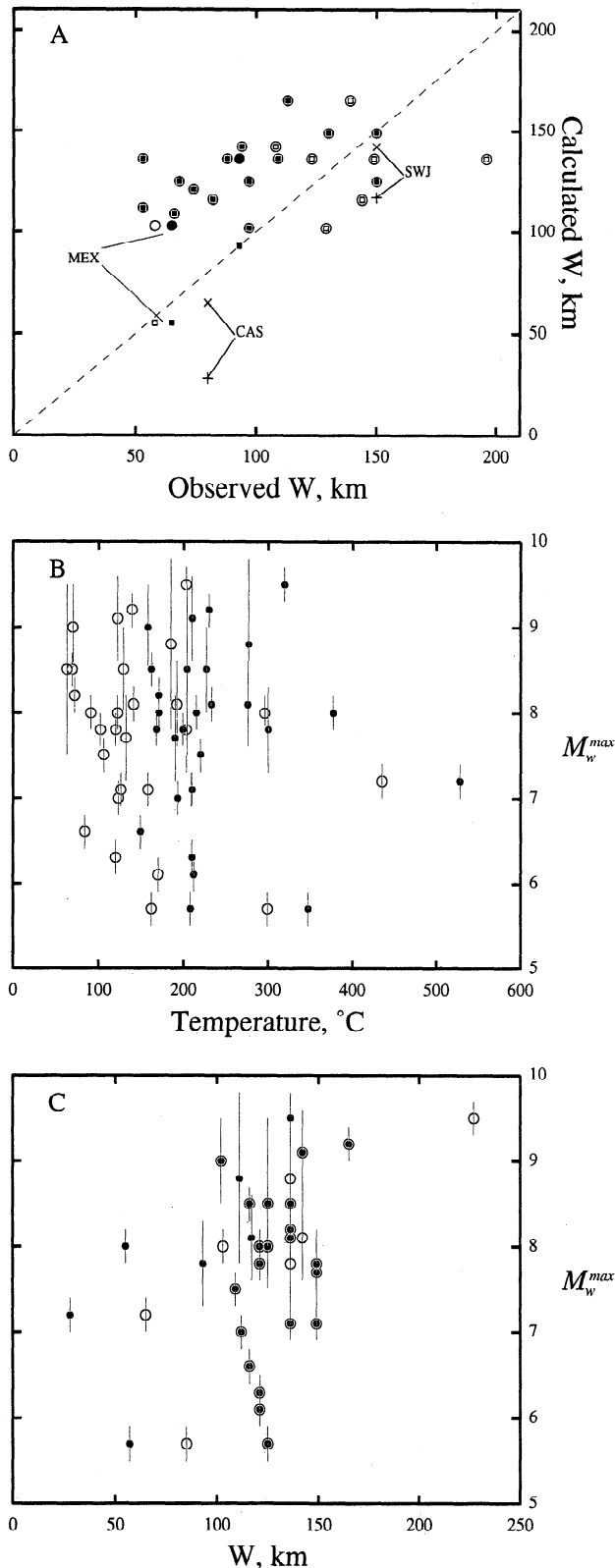
Figure 5. (a) W estimated from earthquakes depths and geodetic data plotted against W estimated from (5) and T_c = 350°C, based on the average lithosphere age, trench-normal convergence rate and dip angle at each trench. Solid symbols are from Pacheco et al. [1993] and open symbols are from Tichelaar and Ruff [1993]. Circles are temperatures without shear heating and squares include heating from 20 MPa stress. The crosses (no stress) and pluses (20 MPa stress) are from CAS [Hyndman and Wang 1993] and SW Japan (SWJ) [Hyndman et al., 1995] as labeled. All data are shown in Table 4. Estimated average temperature (b) and W (c) plotted against observed maximum earthquake size at each subduction thrust fault. Open symbols are temperatures and W without shear heating, and solid symbols include heating from 20 MPa stress. Where open and solid symbols overlap in Figure 5c, the critical temperature is reached below 60 km depth with and without shear heating.
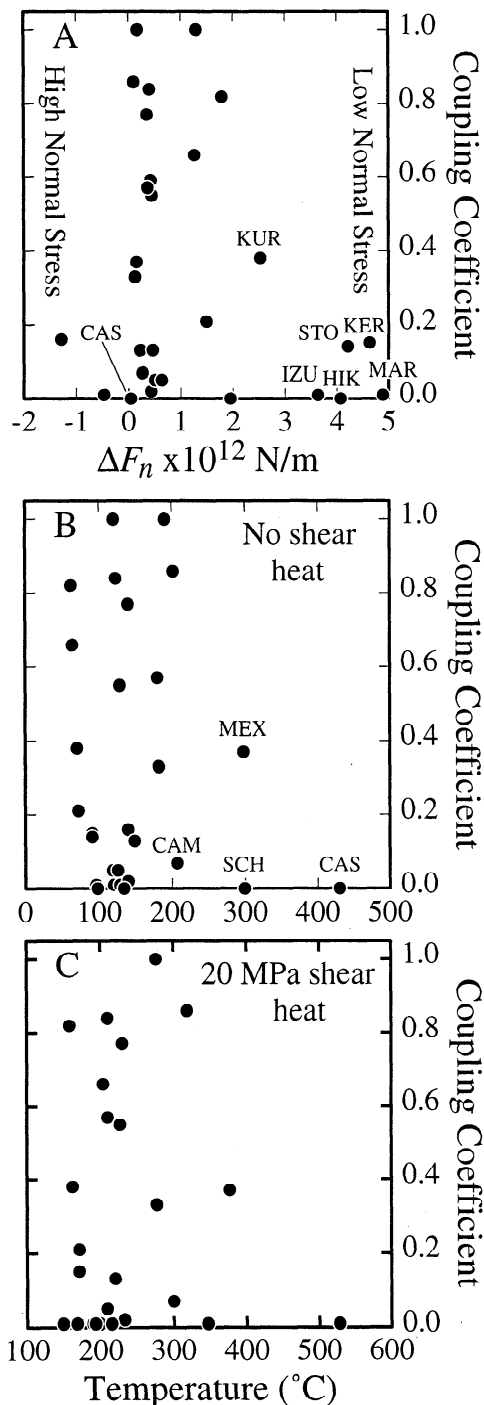
Figure 6. (a) Change in normal stress (per unit length) on subduction thrust faults from slab anchor model of *Scholz and Campos* [1995] plotted against seismic coupling coefficients from *Pacheco et al.* [1993]. (b) Inferred average temperature on the subduction thrust faults plotted against the same seismic coupling coefficients without shear heating. (c) Temperatures including 20 MPa shear heating. Abbreviations given in Table 1.

two (moderate-sized) thrust events, the *Pacheco and Sykes* [1992] catalog contains none, and there is no known history of great quakes [*Richter*, 1958]. The Mexico and Central America subduction zones have anomalous behavior in that they produce many quakes of $M_w \leq 8.0$ but not larger. Mexico and Central America have a combined χ of about 0.2 and so either

they are storing a large slip deficit or have a large component of aseismic slip. Mexico may be transitional between coupled and thermally uncoupled subduction in that it has small quakes, a shallow maximum extent of coupling [*Tichelaar and Ruff*, 1993], and a low coupling coefficient. I suggest that the seismic quiescence of Cascadia is not anomalous when compared to its closest thermal analogs and that it may have a large component of aseismic slip.

The suggestion that the Cascadia subduction zone is largely aseismic may seemingly be at odds with evidence for geologically rapid subsidence events, tsunamis, and present-day strain accumulation [*Mitchell et al.*, 1994]. Such a contradiction may be resolved if the Cascadia subduction fault does not rupture solely in the form of rapid earthquakes but instead has some large but unknown component of slow slip. By slow, I mean rupture that takes several minutes to months instead of seconds and thus does not produce high-frequency seismic waves. Recent slow quakes along the San Andreas were detected only by strain meters [*Linde et al.*, 1996], and other suspected quakes are "silent", that is, seen only in very long-period seismic data [*Beroza and Jordan*, 1990]. Global Positioning System (GPS) measurements from Japan show similar amounts of fast (seismic) and post seismic slow slip from a recent $M_w = 7.6$ subduction event [*Heki et al.*, 1997] while a more recent possible $M_w \approx 6.3$ event occurred entirely by slow slip [*Sagiya*, 1997]. The increasing observations of slow events, that are possible due to technological advances, and the global average of the seismic coupling coefficient of 0.3 [*McCaffrey*, 1997] may be showing that slow slip predominates at subduction zones.

Slow earthquakes can be tsunamigenic. The 1960 Chile $M_w = 9.5$ event began with a 20 min duration "slow" quake with 5 to 10 min period waves [*Kanamori and Cipar*, 1974] and an estimated seismic moment that accounted for about one third
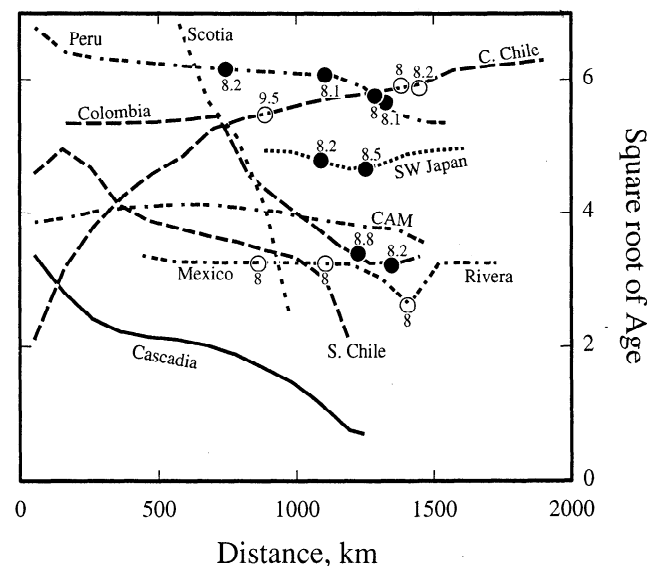

Figure 7. Square root of the age of subducting oceanic lithosphere along the world's youngest subduction zones (distance axis is positive in direction faced if hanging wall is to observer's right and is offset arbitrarily for clarity). Circles show where $M_w \geq 8$ (labeled by magnitude) earthquakes have occurred along each trench (open and solid symbols used only for clarity). Cascadia has the longest stretch of the youngest subducting lithosphere in the world. CAM, Central America.

of the total moment for that event [*Cifuentes and Silver*, 1989]. The low-frequency precursor apparently produced a large tsunami (see Appendix). Similarly, the 1992 Nicaragua slow subduction event produced a large tsunami but relatively little high-frequency seismic energy [*Ide et al.*, 1993].

While the section of the Central Chile trench where the 1960 event occurred (37°S to 47°S) is often compared to Cascadia [*Heaton and Hartzell*, 1987; *Rogers*, 1988], subduction at Central Chile is twice as fast and the subducting lithosphere is on average twice as old (Figure 7), resulting in cooler average temperatures along the plate interface (Table 4). While the mechanics of slow rupture are not understood, one might expect that such behavior is enhanced by high temperature and that Cascadia is as likely a place as any for this to occur. Based on its seismic moment only, if a slow quake the size of the 1960 Chile long-period precursor occurred on the Cascadia subduction zone, it would account for hundreds of years of subduction. Because slow slip is also associated with stress drop, it should produce geologically rapid deformation of the upper plate. However, vertical displacements estimated from paleoseismic observations alone would place little constraint on the size of the seismic portion of the event.

Estimates of Cascadia earthquake potential have focused on the maximum earthquake size for important social reasons, but we might also consider other possibilities that can account for the observations. Amplitudes of the coastal subsidence events are not well known but could be of the order of a meter, consistent with the present maximum coastal uplift rate of 4 mm/yr [*Mitchell et al.*, 1994] and a 300 year repeat time. *Hyndman and Wang*'s [1995] geodetic estimate of plate coupling at Cascadia is a maximum because they assumed full coupling out to the trench. However, the same on-land uplift rate data can be satisfied with as little as 20% of the convergence contributing to upper plate strain (model E, Figure 8), that is, up to 80% of the 40 mm/yr convergence may occur without any increase in stress across the fault. If so, the 300-year Cascadia event need only involve an average of about 2 m of combined rapid and slow slip on the dipping thrust interface. If this slip event was entirely rapid and propagated 100 km along strike (a typical distance for a 2 m slip event) it would be a $M_w = 7.8$ quake. Rupture of the entire margin would produce a $M_w = 8.5$ quake (using a length of 1000 km from Mendocino triple junction to the Nootka fault and a downdip width of 80 km for the locked fault). These "seismic" events will be smaller if some part of the slip is taken up by slow processes. The tsunami observed in Japan is a possible constraint on the amount of slip during the event 300 years ago if it can be convincingly linked to Cascadia [*Satake et al.*, 1996] but offers limited constraint on the duration of the slip.

Conclusions

The distributions of large thrust earthquakes at subduction zones are examined from recurrence, mechanical and thermal points of view with a focus on the effects of relative plate convergence rate and subducting plate age. Earthquake behavior shows a dependence on convergence rate because faster slip decreases the recurrence times of earthquakes. The numbers of quakes of $M_w \geq 7$ in this century and $M_w \geq 6$ in the past 19.3 years as distributed with rate and plate age are also consistent with the recurrence model and mimic the non-uniform distribution of rates and ages at the worlds subduction zones. The
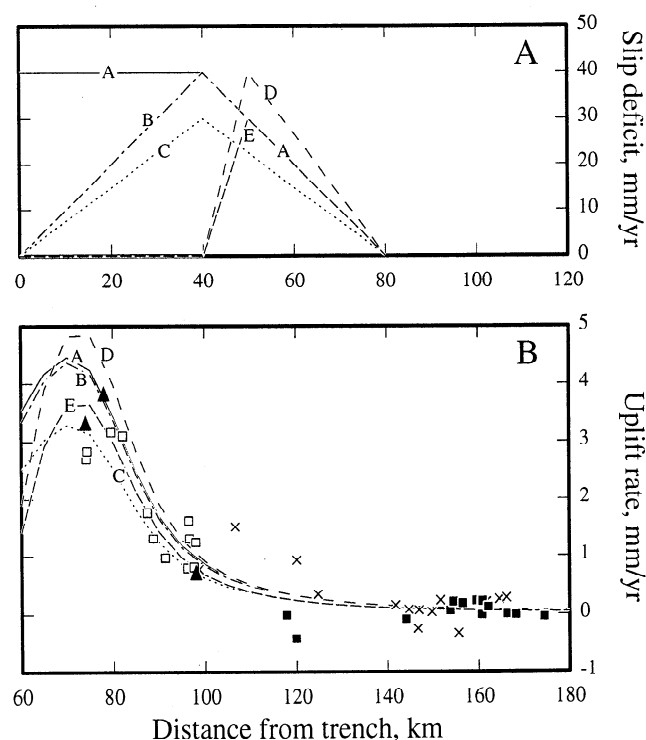

Figure 8. (a) Models of plate locking for the Cascadia subduction zone off southern Oregon and (b) their resulting onshore uplift rates. This figure is used as an example to show that very little coupling is required to satisfy onshore geodetic data, which holds true for most of the Cascadia margin. Possible distributions of slip deficit (convergence rate minus aseismic slip rate) are shown with distance inland from trench. A is the 40-40 model of *Hyndman and Wang* [1995] in which the plate boundary is fully locked for the first 40 km downdip from the trench and decreases linearly to no locking over the next 40 km. This produces the coastal uplift rates shown by curve A in (b). Other inferred locking distributions shown by curves B through E give uplift rates also consistent with the geodetic data. Model E, for example, has only 19% of the convergence locked. Data are from *Mitchell et al.* [1994] and *Hyndman and Wang* [1995] (triangles, tide gauges at Charleston, Crescent City, and Newport in order of increasing distance; squares, Bandon to Coquille leveling line, crosses, Coquille to Dillard line, squares, Newport to Albany line).

slopes of the *Ruff and Kanamori* [1980] and *Kanamori* [1983] regressions that relate maximum earthquake size to convergence rate are also predictable from the recurrence relation. Revised age-rate-M_w^{max} data are better explained with a logarithm of rate relationship, predicted from recurrence times, if the New Hebrides and Tonga trenches, with their fast rates, are given importance. The revised data show no general correlation of M_w^{max} to subducting plate age. The seismic coupling coefficient shows similar agreement with inferred temperature on the thrust fault as it does with the change in normal stress across the plate boundary in the slab anchor model of *Scholz and Campos* [1995]. Finally, from a thermal point of view, Cascadia falls in the category of aseismic plate boundaries rather than a coupled one as predicted by mechanical subduction models. Cascadia is far warmer than any other subduction zone and may be a good place to look for significant aseismic slip.

Appendix

Trench Data

The geographic locations of each trench were taken at an interval of approximately 10 to 15 km from the digital seafloor data DBDB5 and smoothed. At each point the relative plate convergence vector and the age of the subducting lithosphere were calculated. Convergence rates at most trenches are taken from NUVEL-1A rotation poles [DeMets et al., 1994]. Rates at trenches surrounding the Philippine Sea plate are poorly known, yet recent GPS measurements indicate that the Seno et al. [1993] poles may provide rates within 20% of true values (discussed by McCaffrey [1996]). Rates were calculated from poles of rotation that satisfy GPS measurements at Tonga [Bevis et al., 1995] and New Hebrides [Calmant et al., 1995]. The pole for Cascadia is taken from Wilson [1993] and De-Mets et al. [1994]. Plate motion vectors for the Scotia trench are from Pelayo and Wiens [1989].

Subducting plate ages were taken mostly from the compiled grid of Mueller et al. [1993], either by interpolation between nearby grid points or by finding the closest grid point within 200 km of the trench point. In cases where ages are not available from the grid, approximate ages were assigned based on the map of Cande et al. [1989] (Table A1). This precludes detailed analysis of variation with age for older subduction zones but does not affect conclusions regarding the differences between young (i.e., <60 Ma) and old (>80 Ma) ones. For lithosphere produced in the Cretaceous magnetic quiet zone (84 to 118 Ma), ages of 100±20 Ma have been assigned. In the western Aleutians and Kamchatka subduction zones, where the only constraint is that the subducting lithosphere is Cretaceous or older, an age of 115±35 Ma was assigned. These sections, mostly > 80 Ma in age, form less than 20% of the total trench length and have little impact on the conclusions.

Trench averages of age and rate were estimated from discretized samples along the trenches. X_{ij} is the location of the ith digitized point at trench j; D_{ij} is the distance from X_{ij} to $X_{i-1,j}$; A_{ij} is the subducting lithosphere age at X_{ij}; and R_{ij} is the plate convergence rate at X_{ij}. The length of the trench L_j is

$\Sigma_i D_{ij}$, the average age is $\Sigma_i A_{ij} D_{ij} / L_j$, and the average convergence rate is $\Sigma_i R_{ij} D_{ij} / L_j$. Trench lengths are binned by convergence rate and age at 5 mm/yr and 5 Ma increments to produce Table 2; $L(k,m) = \Sigma_{ij} D_{ij}$, where $k=int(A_{ij}/5)+1$, $m=int(R_{ij}/5)+1$, summations are over both i and j. The histogram for age, for example, is then calculated by summing L over all rates for each age range. The age of the lithosphere and rate of convergence at Q_{qj}, the epicenter of earthquake q at trench j, is taken from the trench point X_{ij} that is closest to Q_{qj}. The standard deviations listed in Table 1 for convergence rates, ages, and dips reflect variations in these parameters along the subduction zones more than uncertainties in the values themselves.

Rivera Trench

At the north end of the Mexico trench there is a high level of seismicity associated with the Cocos - Rivera - North America triple junction, including $M_w \approx 8$ quakes in 1932 [Singh et al., 1985] and 1995 [Courboulex et al., 1997]. Both of these earthquakes nucleated within the subducting and broadly deforming Cocos - Rivera plate boundary [DeMets and Wilson, 1997] and propagated to the NW into the Rivera subduction zone. Hence they are probably not a good test of the influence of temperature alone and the Rivera trench is grouped with the Mexico trench. The subducting plate age at the Rivera trench is from DeMets and Wilson [1997].

1960 Chile Tsunami

According to Cifuentes and Silver [1989], the main shock of the May 22 Chile event was preceded by a 1150 s long slow precursor. The main shock origin time was 1911:30 UT and therefore the precursor origin time was about 1852:20 UT. The tide gauge at Talcahuano (≈36.8°S), within 100 km of the epicenter, shows a clear large amplitude signal starting prior to 1900 UT [Japan Meteorological Agency 1961], suggesting the low-frequency precursor was tsunamigenic. This tsunami was probably not due to a $M_s = 7.8$ quake at 1855:57 UT [Cifuentes 1989] because its amplitude was much larger than that due to a closer $M_s = 8.3$ event the preceding day.

Seismic Coupling Coefficients

Seismic coupling coefficients are taken from Petersen and Seno [1984] and Pacheco et al. [1993]. In their estimates of χ, Scholz and Campos [1995] include large earthquakes of the 19th century at some subduction zones, thereby increasing χ. The pitfalls of including 19th century quakes are that the earthquake data set becomes heterogeneous in time and that there is at least an order of magnitude uncertainty in the seismic moments for 19th century quakes, which are based on written accounts of earthquake effects. For example, a conservative factor of 2 uncertainty in each of length, width and slip results in a factor of 8 uncertainty in the seismic moment. Consider also that the uncertainty in seismic moment for the 1960 Chile earthquake is still a factor of 2, although it is based on instrumental recordings [Cifuentes and Silver, 1989] rather than descriptions of the quake's effects. Given that the useful range of χ is over only 1 magnitude order (0.1 to 1.0), data that have order-of-magnitude uncertainty do not add information. The revisions of Scholz and Campos [1995] are not used here but make little difference on the conclusions.

Table A1. Sections of Trenches with Poorly Constrained Ages

Trench	Section of Trench	Age, Ma	Notes
W. Aleutian	164°E to 169.5°E	100±20	At least 80 Ma, oldest Emperor Seamount; likely CQZ
Aleutian	169.5°E to 175°E	48±4	Lonsdale [1988]; anomalies 19 to 22
Izu-Bonin	24°N to 27°N	150±20	near M18 to M22
Java	104°E to 114°E	100±20	CQZ
Kuriles	44°N to 48°N	127±5	M1 to southeast
Kamchatka	48°N to 54.6°N	115±35	Mesozoic to SE, or CQZ
New Hebrides	18°S to 22°S	45±5	40 to 50 Ma to south
Tonga-Kermadec-New Zealand	14°S to 43°S	100±20	CQZ; at least 70 Ma at Osborne Seamount

CQZ, Cretaceous magnetic quiet zone (80 to 115 Ma).

Notation

κ	thermal diffusivity, 10^{-6} m^2/s.
k	thermal conductivity, 3.3 W m^{-1}°K^{-1}.
μ	shear modulus, 4×10^{10} N/m^2.
χ	seismic coupling coefficient.
β	slope of $\log(N)$ versus $\log(M_o)$, 2/3.
σ	shear stress on thrust fault, 20 MPa.
A	subducting plate age.
v	subduction convergence rate.
v_n	trench-normal convergence rate.
L	trench length.
W	downdip length of seismogenic plate boundary.
δ	dip angle of thrust fault.
τ	time.
M_o^{max}	moment of largest possible earthquake at trench.
M_w^{max}	magnitude of largest observed earthquake at trench.
T	recurrence time for earthquake.
c_v	slope of M_w^{max} versus v relation.
c_a	slope of M_w^{max} versus A relation.
T_f	temperature on thrust fault.
z_f	depth on thrust fault.
T_o	initial mantle temperature, 1350°C.
b	constant close to unity, from Table 1 of *Molnar and England* [1995].
T_c	critical temperature above which the fault slides stably, 350°C.

References

Atwater, B.F., Geologic evidence for earthquakes during the past 2000 years along the Copalis River, southern coastal Washington, *J. Geophys. Res.*, *97*, 1901-1919, 1992.

Beroza, G.C., and T.H. Jordan, Searching for slow and silent earthquakes using free oscillations, *J. Geophys. Res.*, *95*, 2485-2510, 1990.

Bevis, M., et al., Geodetic observations of very rapid convergence and back-arc extension at the Tonga island arc, *Nature*, *374*, 249-251, 1995.

Byrne, D.E., D.M. Davis, and L.R. Sykes, Loci and maximum size of thrust earthquakes and the mechanics of the shallow region of the subduction zone, *Tectonics*, *7*, 833-857, 1988.

Calmant, S., P. Lebellegard, F. Taylor, M. Bevis, D. Maillard, J. Recy, and J. Bonneau, Geodetic measurements of convergence across the New Hebrides subduction zone, *Geophys. Res. Lett.*, *22*, 2573-2576, 1995.

Cande, S.C., J.L. LaBreque, R.L. Larson, W.C. Pitman, X. Golovchenko, and W.F. Haxby, Magnetic lineations of the world's ocean basins, 1:27,400,000, Am. Assoc. of Pet. Geol., Tulsa, Okla., 1989.

Carslaw, H.S., and J.C. Jaeger, *Conduction of Heat in Solids*, 510 pp., Oxford Univ. Press, New York, 1959.

Cifuentes, I., The 1960 Chilean earthquakes, *J. Geophys. Res.*, *94*, 665-680, 1989.

Cifuentes, I., and P. Silver, Low-frequency source characteristics of the great 1960 Chilean earthquake, *J. Geophys. Res.*, *94*, 643-663, 1989.

Courboulex, F., S.K. Singh, J.F. Pacheco, and C.J. Ammon, The 1995 Colima-Jalisco, Mexico, earthquake (Mw 8): A study of the rupture process, *Geophys. Res. Lett.*, *24*, 1019-1022, 1997.

DeMets, C., and D.S. Wilson, Relative motions of the Pacific, North American, and Cocos plates since 0.78 Ma, *J. Geophys. Res.*, *102*, 2789-2806, 1997.

DeMets, C., R.G. Gordon, D.F. Argus, and S. Stein, Effects of recent revisions to the geomagnetic reversal time scale on estimates of current plate motions, *Geophys. Res. Lett.*, *21*, 2191-2194, 1994.

Dziewonski, A.M., T.-A. Chou, and J.H. Woodhouse, Determination of earthquake source parameters from waveform data for studies of global and regional seismicity, *J. Geophys. Res.*, *86*, 2825-2852, 1981.

Hagerty, M.T., and S.Y. Schwartz, The 1992 Cape Mendocino earthquake: Broadband determination of source parameters, *J. Geophys. Res.*, *101*, 16043-16058, 1996.

Hanks, T.C., and H. Kanamori, A moment magnitude scale, *J. Geophys. Res.*, *84*, 2348-2350, 1979.

Heaton, T.H., and S.H. Hartzell, Earthquake hazards on the Cascadia subduction zone, *Science*, *236*, 162-168, 1987.

Heaton, T.H., and H. Kanamori, Seismic potential associated with subduction in the northwestern United States, *Bull. Seismol. Soc. Am.*, *74*, 933-941, 1984.

Heki, K., S. Miyazaki, and H. Tsuji, Silent fault slip following an interplate thrust earthquake at the Japan trench, *Nature*, *386*, 595-598, 1997.

Hyndman, R.D., and K. Wang, Thermal constraints on the zone of major thrust earthquake failure: The Cascadia Subduction Zone, *J. Geophys. Res.*, *98*, 2039-2060, 1993.

Hyndman, R.D., and K. Wang, The rupture zone of Cascadia great earthquakes from current deformation and the thermal regime, *J. Geophys. Res.*, *100*, 22133-22154, 1995.

Hyndman, R.D., K. Wang, and M. Yamano, Thermal constraints on the seismogenic portion of the southwestern Japan subduction thrust, *J. Geophys. Res.*, *100*, 15373-15392, 1995.

Ide, S., F. Imamura, Y. Yoshida, and K. Abe, Source characteristics of the Nicaraguan tsunami earthquake of September 2, 1992, *Geophys. Res. Lett.*, *20*, 863-866, 1993.

Japan Meteorological Agency, The report on the tsunami of the Chilean earthquake, 1960 (in Japanese), *Tech. Rep. 8*, pp. 217-225, March 1961.

Jarrard, R.D., Relations among subduction parameters, *Rev. Geophys*, *24*, 217-284, 1986.

Kagan, Y.Y., Seismic moment-frequency relation for shallow earthquakes: Regional comparison, *J. Geophys. Res.*, *102*, 2835-2852, 1997.

Kanamori, H., Global seismicity, in *Earthquakes: Observation, Theory and Interpretation*, edited by H. Kanamori and E Boschi, 597-608, North-Holland, New York, 1983.

Kanamori, H., Rupture process of subduction-zone earthquakes, *Annu. Rev. Earth Planet. Sci.*, *14*, 293-322, 1986.

Kanamori, H., and J. Cipar, Focal process of the great Chilean earthquake May 22, 1960, *Phys. Earth Planet. Inter.*, *9*, 128-136, 1974.

Lay, T., and T.C. Wallace, *Modern Global Seismology*, Academic, San Diego, Calif., 1995.

Linde, A.T., M.T. Gladwin, M.J.S. Johnston, R.L. Gwyther, and R.G. Bilham, A slow earthquake sequence on the San Andreas fault, *Nature*, *383*, 65-68, 1996.

Lonsdale, P., Paleogene history of the Kula plate: Offshore evidence and onshore implications, *Geol. Soc. Am. Bull.*, *100*, 733-754, 1988.

McCaffrey, R., Dependence of earthquake size distributions on convergence rates at subduction zones, *Geophys. Res. Lett.*, *21*, 2327-2330, 1994.

McCaffrey, R., Slip partitioning at convergent plate boundaries of SE Asia, in *Tectonic Evolution of SE Asia Symposium, Geol. Soc. Spec. Publ.*, *106*, 3-18, 1996.

McCaffrey, R., Statistical significance of the seismic coupling coefficient, *Bull. Seismol. Soc. Am.*, in press, 1997.

Mitchell, C.E., P. Vincent, R.J. Weldon II, and M.A. Richards, Present-day vertical deformation of the Cascadia margin, Pacific Northwest, U.S.A., *J. Geophys. Res.*, *99*, 12257-12277, 1994.

Molnar, P., Earthquake recurrence intervals and plate tectonics, *Bull. Seismol. Soc. Am.*, *69*, 115-133, 1979.

Molnar, P., and P. England, Temperatures in zones of steady-state underthrusting of young oceanic lithosphere, *Earth Planet. Sci. Lett.*, *131*, 57-70, 1995.

Mueller, R.D., W.R. Roest, J.-Y. Royer, L.M. Gahagan, and J.G. Sclater, A digital map of the ocean floor, *SIO Ref. Ser. 93-30*, Scripps Inst. of Oceanog., La Jolla, Calif., 1993.

Nelson, A., et al., Radiocarbon evidence for extensive plate-boundary

rupture about 300 years ago at the Cascadia subduction zone, *Nature, 378,* 371-374, 1995.

Pacheco, J.F., and L.R. Sykes, Seismic moment catalog of large shallow earthquakes, 1900 to 1989, *Bull. Seismol. Soc. Am., 82,* 1306-1349, 1992.

Pacheco, J.F., L.R. Sykes, and C.H. Scholz, Nature of seismic coupling along simple plate boundaries of the subduction type, *J. Geophys. Res., 98,* 14133-14159, 1993.

Peacock, S.M., Thermal and petrologic structure of subduction zones, in *Subduction: Top to Bottom, Geophys. Monogr. Ser.* vol. 96, edited by G. E. Bebout et al., pp. 119-133, AGU, Washington D.C., 1996.

Pelayo, A.M., and D.A. Wiens, Seismotectonics and relative plate motions in the Scotia Sea region, *J. Geophys. Res., 94,* 7293-7320, 1989.

Peterson, E.T., and T. Seno, Factors affecting seismic moment release rates in subduction zones, *J. Geophys. Res., 89,* 10233-10248, 1984.

Richter, C.F., *Elementary Seismology,* 768 pp., W.H. Freeman, New York, 1958.

Rogers, G.C., An assessment of the megathrust earthquake potential of the Cascadia subduction zone, *Can. J. Earth Sci., 25,* 844-852, 1988.

Rundle, J.B., Derivation of the complete Gutenberg-Richter magnitude-frequency relation using the principle of scale invariance, *J. Geophys. Res. 94,* 12337-12342, 1989.

Ruff, L., and H. Kanamori, Seismicity and the subduction process, *Phys. Earth Planet. Inter., 23,* 240-252, 1980.

Sagiya, T., Anomalous transients in crustal movements of the Boso Peninsula, Japan - Is it a slow earthquake?, *EOS, Trans. Amer. Geophys. Un., 78,* S214, 1997.

Satake, K., K. Shimazaki, Y. Tsuji, and K. Ueda, Time and size of a giant earthquake in Cascadia inferred from Japanese tsunami records of January 1700, *Nature, 379,* 246-249, 1996.

Scholz, C.H., *The Mechanics of Earthquakes and Faulting,* 439 pp., Cambridge Univ. Press, New York, 1990.

Scholz, C.H., and J. Campos, On the mechanism of seismic decoupling and backarc spreading at subduction zones, *J. Geophys. Res., 100,* 22103-22115, 1995.

Seno, T., S. Stein, and A. Gripp, A model for the motion of the Philippine Sea plate consistent with NUVEL-1 and geological data, *J. Geophys. Res., 98,* 17941-17948, 1993.

Singh, S.K., L. Ponce, and S. P Nishenko, The great Jalisco, Mexico, earthquakes of 1932: Subduction of the Rivera plate, *Bull. Seismol. Soc. Am. 75,* 1301-1314, 1985.

Stesky, R., W. Brace, D. Riley, and P.Y. Robin, Friction in faulted rock at high temperature and pressure, *Tectonophysics, 23,* 177-203, 1974.

Tanioka, Y., K. Satake, and L. Ruff, Seismotectonics of the April 25, 1992, Petrolia earthquake and the Mendocino triple junction region, *Tectonics, 14,* 1095-1103, 1995.

Tichelaar, B.W., Depth of seismic coupling along subduction zones, Ph.D. thesis, 235 pp., Univ. of Mich., Ann Arbor, 1991.

Tichelaar, B.W., and L.J. Ruff, Depth of seismic coupling along subduction zones, *J. Geophys. Res., 98,* 2017-2037, 1993.

Tse, S.T., and J.R. Rice, Crustal earthquake instability in relation to the depth variation of frictional slip properties, *J. Geophys. Res., 91,* 9452-9472, 1986.

Uyeda, S., and H. Kanamori, Back-arc opening and the mode of subduction, *J. Geophys. Res., 84,* 1049-1061, 1979.

Wilson, D.S., Confidence intervals for motion and deformation of the Juan de Fuca plate, *J. Geophys. Res., 98,* 16053-16071, 1993.

Wyss, M., Toward a physical understanding of the earthquake frequency distribution, *Geophys. J. R. Astron. Soc., 31,* 341-360, 1973.

R. McCaffrey, Department of Earth and Environmental Sciences, Rensselaer Polytechnic Institute, Troy, NY 12180-3590 (e-mail: robmcc@geo.rpi.edu)